Ultimate failure load analysis of cross-laminated timber panels subjected to in-plane compression

Markku Heinisuo, Sami Pajunen [*], Aku Aspila

Tampere University, Finland

ABSTRACT

Cross-laminated timber (CLT) panels have proved their efficiency as vertical and horizontal load-carrying structures, and their design methods for serviceability and ultimate limit states are well defined. However, there is a lack of more general and versatile analytical methods for the ultimate load carrying capacity determination of CLT structures. In this paper, the classical layered beam theory is adopted for the ultimate failure load estimation of axially compressed CLT panels. The proposed method retains its accuracy both with an asymmetric layer setup and when the number of CLT layers exceeds five. The presented method is validated by adopting experimental test data from two test series produced by other researchers.

1. Introduction

Cross-laminated timber (CLT) is increasingly used in planar and volumetric construction elements due to its many favorable properties, such as high in-plane and out-of-plane strength and stiffness. Typical applications of CLT are in mid- and high-rise timber buildings as load-bearing walls and slabs. Typically, the slab design is driven by out-of-plane bending. In the wall design, the primary loads are in-plane compression and shear, whereas bending is of lesser importance. Nowadays, design and analysis methods for CLT structures are available in many national design guides [1,2]. Additionally, the forthcoming Eurocode 5 will also consider the design of CLT structures. The most widely used methods for CLT panels supported on two sides are the Timoshenko beam theory [3], the gamma method [4], and the Shear Analogy method [5]. On the other hand, if the CLT panel is supported on three or four sides, the design can be based on finite element method applications [6], simplified rules based on plate theory [1], or some other approximative approaches.

Current design methods [1,2] for eccentrically compressed CLT panels are based on the well-known Ayrton Perry theory. Recently, a refined method, that considers the shear deformations in transverse layers more accurately is presented [17]. However, all these methods are limited to certain loading and boundary conditions, and they can not predict the ultimate failure load with arbitrary loading and boundary conditions. Hence, more general design method for compressed CLT panels is needed.

In this paper, the classical theory of layered beams (TLB) is applied to the ultimate failure load analysis of CLT panels subjected to concentric and eccentric axial in-plane compression loads. Shear and bending-dominated load cases are thus outside of the scope of this paper. Related to the above-mentioned three common methods, the TLB has the same theoretical basis as the Shear Analogy method [7]. The layered beam theory was derived during the late 1940 s [8–12], and since then it has proven to be an accurate and efficient analysis method for various layered structures, such as sandwich beams [13,14]. The TLB can be applied also to CLT structures with an arbitrary number of layers with arbitrary material properties and thicknesses [7]. This is a great benefit when compared to the widely used gamma method, which loses its accuracy when the number of layers exceeds five. In the TLB, beam deflection is governed by a sixth-order differential equation. If the beam is supported and loaded simply enough, the governing differential equation can be solved analytically. In more complicated cases, an exact finite element formulation with related matrix analysis can be used to solve the differential equation [15]. When the TLB is applied to axially compressed CLT structures, the following two assumptions are made. Firstly, following the standard argumentation, the normal stresses are assumed to behave in a linearly elastic manner until the point of failure. To be precise, such an assumption is not exact for wood material [16]. Nevertheless, the results are accurate enough for structural timber design and analysis. Secondly, the rolling shear stresses in the transverse layers are also assumed to be linearly elastic up to the point of failure. This assumption is based on experimental results of similar compressed

CLT panels [17].

The paper is organized as follows: after the introduction, the TLB is applied to compressed CLT panels, and essential analytical solutions are presented in Chapter 2. In Chapter 3, the TLB is augmented to estimate the ultimate failure load, followed by the method validation in Chapter 4 using tests published in [17,18]. Finally, in Chapter 5, conclusions are drawn and recommendations for the use of the proposed method are given.

2. Classical theory of layered beams applied to CLT beams

The analysis of CLT beams is traditionally carried out by using simple analytical approaches such as the gamma method or the Shear Analogy method. In addition to these two simple methods, the finite element method (FEM) can also be utilized either by adopting the Timoshenko beam theory or orthotropic plate theories with advanced material models. However, the classical theory of layered beams represents a general and accurate method, which lies between the simple analytical approaches and laborious numerical methods. The TLB is applied to the out-of-plane bending analysis of CLT beams in [7], and in the current paper, the theory is utilized in the analysis of CLT beams subjected primarily to axial loading. Moreover, the theory is also augmented with the determination of the ultimate failure load of the axially loaded CLT beams.

The main assumption in the classical theory of layered beams is the so-called generalized Euler-Bernoulli hypothesis, according to which the centroids of parallel layers remain in the same line when the beam is subjected to bending. This is a looser assumption compared to the conventional Euler-Bernoulli beam theory, which assumes that the entire cross-section remains plane under bending. By the definition of the layered beam theory, the parallel layers are those where the grain orientation is parallel to the longitudinal axis of the beam. In the TLB, these parallel layers are called *faces*. As shown in [7], the generalized Euler-Bernoulli assumption is exactly true only for certain cross-sections, and otherwise the assumption is valid approximatively. For example, the assumption is exactly true for symmetric three- and five-layer CLT cross-sections, but the assumption is approximatively true for cross-sections with seven layers. However, the resulting errors remain small.

In a typical CLT configuration, the layers perpendicular to the parallel ones are called transversal layers or more generally *cores* in the layered beam. Following the standard procedure, the transversal layers deform only due to shear force, whereas the parallel layers deform only due to the cross-section bending moment. Such kinematics are well reasoned for CLT beams due to low rolling shear stiffness in the transversal layers. Moreover, it is assumed that the bonding between faces and cores is ideally stiff and strong enough so that the CLT cross-section can fulfill the generalized Euler-Bernoulli hypothesis. In what follows, let us consider a general CLT beam cross-section with the notations depicted in Fig. 1.

The physical meaning of the parameters in Fig. 1 is as follows. M_i denotes the moment of layer i with respect to the centroid of the cross-section of the layer i. M_0 denotes the sum of the bending moments M_i and M_s denotes the sum of the bending moments of the axial forces N_i of the layers i with respect to the centroid of the entire cross-section. Similarly, Q_i denotes the shear force of the layer i. Q_0 denotes the sum of the shear forces Q_i and Q_s denotes the sum of the shear forces of the transverse layers j.

Following the standard reasoning [15], the above-mentioned kinematic assumptions result in a sixth-order differential equation for the beam axis deflection $v(x)$ taking into account the 2nd order effects as

$$B_0 B_s v^{(6)} - (Bk + NB_s)v^{(4)} + Nkv^{(2)} = B_s p^{(2)} - kp \qquad (1)$$

in which N is the axial force in the beam, $p(x)$ is the distributed load intensity, and $v(x)$ is the deflection of the beam axis. Moreover, the other parameters and variables in (1) are as follows: B_0 is the sum of the bending stiffnesses of n parallel layers (faces) of the cross-section, E_i is the Young's modulus of layer i in the beam axis direction, and I_i is the second moment of the layer i area with respect to the layer's local centroidal axis ($I_i = bh_i^3/12$). Thus, B_0 can be written as

$$B_0 = \sum_{i=1}^{n} E_i I_i. \qquad (2)$$

B_s is the so-called Steiner term of the layer i with respect to the centroidal axis of the whole cross-section, and A_i is the area of layer i ($A_i = bh_i$) so that the term can be written as

$$B_s = \sum_{i=1}^{n} y_i^2 E_i A_i. \qquad (3)$$

B is the sum of these two terms, defining the whole cross-section bending stiffness as

$$B = B_0 + B_s. \qquad (4)$$

Moreover, in the equation (1), the parameter k denotes the shear factor of the CLT cross-section, and it is defined in the layered beam theory as

$$k = \sum_{j=1}^{n-1} a_j^2 k_j, \qquad (5)$$

in which a_j is the distance of the centroids of the adjacent parallel layers on both sides of transverse layer j ($j = 1,\ldots, n$-1) and k_j is the shear stiffness intensity of the transverse layer j. In CLT panels, the shear stiffness intensity of the transverse layer j can be calculated as

$$k_j = \frac{G_j b}{h_j}, \qquad (6)$$

in which b is the width of the CLT cross-section, h_j is the height of the transverse layer j, and G_j is the rolling shear modulus of the transverse
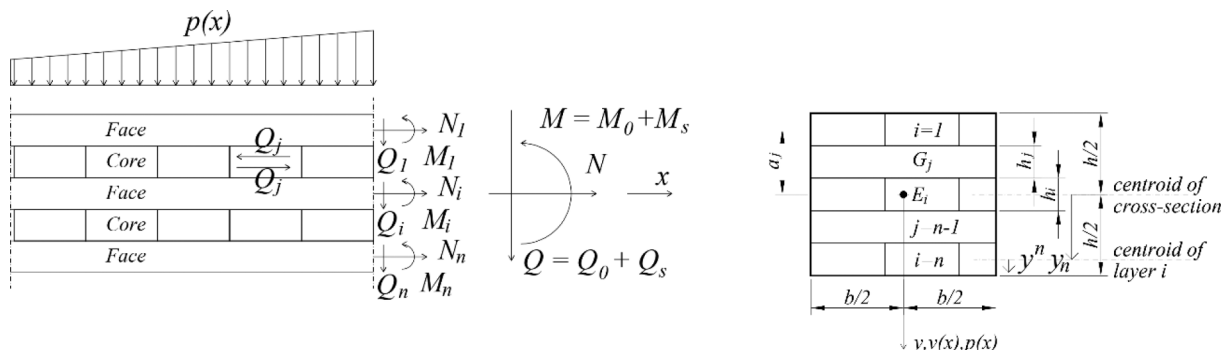

Fig. 1. Stress resultants and cross-section of a CLT beam.

layer *j*.

Being a very general approach, the layered beam theory covers the well-known structural beam analysis cases shown in Table 1.

Complementary boundary conditions of the differential equation (1) can be written generally as

$$Q_y = Q_y^* \quad or \quad v = v^* \tag{7}$$

$$M = M^* \quad or \quad \varphi = \varphi^* \tag{8}$$

$$M_0 = M_0^* \quad or \quad \gamma = \gamma^* \tag{9}$$

in which the asterisk * denotes a given value, and the variables in the boundary conditions can be written more explicitly as

$$Q_y = Q + Nv' \tag{10}$$

$$Q = \sum_{i=1}^{n} Q_i + Q_s = Q_0 + Q_s = -B_0 v''' + k\gamma \tag{11}$$

$$M = \sum_{i=1}^{n} M_i + M_s = M_0 + M_s = -B_0 v'' - B_s v'' + B_s \gamma' = -B v'' + B_s \gamma' \tag{12}$$

$$\varphi = v' - \gamma \tag{13}$$

$$\gamma = -\frac{B_s}{k} \left[-\frac{B_0 v^{(5)}}{k} + \left(1 + \frac{N}{k}\right) v'' + \frac{p'}{k} \right]. \tag{14}$$

In the equations (7)–(12) Q_0 and M_0 denote the sum of shear forces and local bending moments of the separate faces, respectively, Q_s is the sum of shear forces of the cores, and M_s is the bending moment due to the axial stresses of separate face. In the equations (13–14) ϕ denotes the beam neutral axis rotation and γ denotes the slip angle due to core layers' shear deformations.

The differential equation (1) augmented with the boundary conditions (7–9) can be solved in closed form for some elementary cases [14], but the finite element method must be adopted for more complex problems [15]. After solving the differential equation in either way, the shear forces Q_0 and Q_s, bending moments M_0 and M_s, and the slip angle γ can be calculated according to (10–14). After solving the stress resultants, the elastic stress distribution in the cross-section can be defined straightforwardly. The shear stress τ_j of the core j is

$$\tau_j = \frac{T_j}{b} = \frac{k_j a_j}{b}\gamma, \quad j = 1, \cdots, n-1, \tag{15}$$

in which $T_j = k_j a_j \gamma = k_j a_j Q_s/k$ is the shear flow in the core j. In contrast, the conventional Euler-Bernoulli beam theory is adopted for each face leading to parabolic shear stress distribution within each face. Hence, the maximum value of the shear stress in the face i is calculated as

$$\tau_i = -\frac{1.5 E_i I_i}{A_i} v''', \quad i = 1, \ldots, n \tag{16}$$

The axial stress in the face i is calculated from the axial force and bending moments as

$$\sigma_i = \frac{E_i}{\sum_{i=1}^{n} E_i A_i} N + \frac{y^i E_i}{B_0} M_0 + \frac{y_i E_i}{B_s} M_s, \quad i = 1, \cdots, n \tag{17}$$

Table 1
Special cases of the layered beam theory.

Parameter values	Corresponding case
$B_0 = 0$ and $B_s = B$	Timoshenko beam
$k = \infty$	Homogenous Euler-Bernoulli beam
$B_0 = 0$	Thin-faced beam
$k = 0$	Beam with separate faces

in which y^i is the local coordinate of the face i with range $y^i \in [-h_i/2, h_i/2]$.

Based on the TLB fundamentals given above, it can be seen that the central part of the method is the solution of the differential equation (1). Based on the character of the differential equation (1), the solution is sought by using the general solution of the homogenous differential equation for cases $p(x) \equiv 0$, and by using the particular solution of (1) for cases with distributed loads ($p(x) \neq 0$). Solution techniques for these tasks are presented in textbooks on the fundamentals of differential equations. In what follows, no distributed out-of-plane bending loads are considered, and only the use of the homogenous equation general solution is presented.

Let us consider the simply supported beam depicted in Fig. 2. The sliding between layers is prevented in the beam ends and the beam is loaded by an eccentric axial force as shown. The boundary conditions are now

$$v\left(\pm\frac{L}{2}\right) = 0, \; M\left(\pm\frac{L}{2}\right) = -eN, \; \gamma\left(\pm\frac{L}{2}\right) = 0 \tag{18}$$

The solution of the differential equation (1) is in general form

$$v(x) = v_0(x) + v_1(x), \tag{19}$$

in which v_0 is the general solution of the homogenous equation, and v_1 is the particular solution of the whole differential equation. According to [15], the homogenous solution can be found if the compressive axial load fulfills the condition

$$-k\left(\frac{B_o}{B_s} + 1\right) \Big\langle N < 0. \tag{20}$$

It should be noted that [15] states the cases in which the condition (20) is not fulfilled (i.e., $N \leq -k(B_0/B_s + 1)$) are not of practical interest. When (20) is fulfilled, the homogenous solution is

$$v_0(x) = C_1 \cosh\lambda_1 x + C_2 \sinh\lambda_1 x + C_3 \cos\lambda_2 x + C_4 \sin\lambda_2 x + C_5 x + C_6, \tag{21}$$

in which the parameters C_i ($i = 1, \ldots, 6$) are defined according to the boundary conditions (18). Assuming symmetric deflections with respect to the mid-span of the beam, then all the asymmetric terms in (21) must vanish. In other words, $C_2 = C_4 = C_5 = 0$. The first boundary condition (18a): $v(L/2) = 0$ implies

$$C_6 = -C_1 \cosh\frac{\lambda_1 L}{2} - C_3 \cos\frac{\lambda_2 L}{2}. \tag{22}$$

The third boundary condition (18c): $\gamma (L/2) = 0$ implies

$$C_1 = \frac{\lambda_2^3 \sin\frac{\lambda_2 L}{2}\left(-\frac{B_0\lambda_2^2}{k} - 1 - \frac{N}{k}\right)}{\lambda_1^3 \sinh\frac{\lambda_1 L}{2}\left(-\frac{B_0\lambda_1^2}{k} + 1 + \frac{N}{k}\right)} C_3 = \frac{\alpha_4}{\alpha_5} C_3. \tag{23}$$

The second boundary condition (18b): $M(\frac{L}{2}) = -eN$ implies in turn

$$C_3 = \frac{-eN}{-B(\alpha_6 - \alpha_7) + \frac{B_s^2 B_0}{k^2}\left(\lambda_1^4\alpha_6 - \lambda_2^4\alpha_7\right) - \frac{B_s^2}{k}\left(1 + \frac{N}{k}\right)\left(\lambda_1^2\alpha_6 + \lambda_2^2\alpha_7\right)}. \tag{24}$$

In the formulas (22)–(24), the following parameters are used for the sake of clarity

$$\lambda_1 = \sqrt{\frac{1}{2}\left(-\frac{\alpha_2}{\alpha_1} + \sqrt{\frac{\alpha_2^2}{\alpha_1^2} - 4\frac{\alpha_3}{\alpha_1}}\right)}, \; \lambda_2 = \sqrt{\frac{1}{2}\left(\frac{\alpha_2}{\alpha_1} + \sqrt{\frac{\alpha_2^2}{\alpha_1^2} - 4\frac{\alpha_3}{\alpha_1}}\right)} \tag{25}$$

$$\alpha_1 = B_0 B_s, \; \alpha_2 = -(Bk + NB_s), \; \alpha_3 = Nk \tag{26}$$

$$\alpha_6 = \frac{\alpha_4}{\alpha_5}\lambda_1^2\cosh\frac{\lambda_1 L}{2}, \; \alpha_7 = \lambda_2^2\cos\frac{\lambda_2 L}{2} \tag{27}$$

If the presented beam problem boundary conditions are modified so that the sliding between faces is free to occur at the beam ends, we must replace the boundary condition (18c): $\gamma(L/2) = 0$ with a new condition
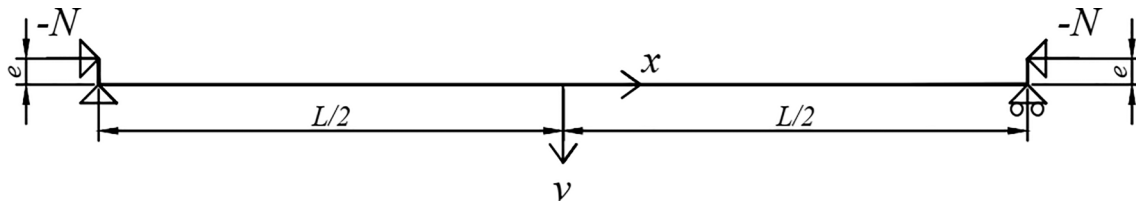
Fig. 2. CLT beam loaded by eccentric axial loads at both ends. The origin of the x-axis is at the mid-span of the beam.

$M_0 (L/2) = 0$. In this case, the homogenous solution parameter C_1 in (23) is then replaced by

$$C_1 = \frac{\lambda_2^2 \cos \frac{\lambda_2 L}{2}}{\lambda_1^2 \cosh \frac{\lambda_1 L}{2}} C_3 = \frac{\alpha_4}{\alpha_5} C_3. \qquad (28)$$

The other equations (22) and (24) for the parameters C_3 and C_6 remain unchanged. The explicit formulas for the bending moments for the considered case are given in the Appendix.

3. Ultimate failure load determination

Based on the theoretical framework presented above and in [7], the theory of layered beams can be utilized for various purposes in the analysis and design of CLT slabs similarly to the widely used gamma method and the Shear Analogy method. However, in this paper, the research focus is on the analysis and especially on the ultimate failure load determination of axially loaded CLT beams. In recent structural loading tests [17], it has been observed that CLT panels subjected primarily to axial compression load tend to lose their load-bearing capacity either by longitudinal tension or compression failure in the outermost lamella. It was also noticed that no rolling shear or other failure modes, which are typical to bending-only load cases, were present in the tests before the point of ultimate failure [17].

Let us augment the axial stress formula (17) with compression and tension constraints so that the following condition must be fulfilled in each face

$$\sigma_c \leq \sigma_i = \frac{E_i}{\sum_{i=1}^{n} E_i A_i} N + \frac{E_i y^i}{B_0} M_0 + \frac{y_i E_i}{B_s} M_s \leq \sigma_t, \quad i = 1, \cdots, n \qquad (29)$$

in which σ_c and σ_t are the compression and tension limit stresses for the elastic phase. In other words, if (29) inequality holds as the equation in either compression or tension, the layer and hence the whole beam has reached the failure state.

Linearization of the wood material stress–strain curve in the longitudinal direction is a standard practice in the analysis and design of timber structures. Moreover, in the case of considered CLT beams, certain non-linear elasticity and plasticity in the longitudinal axial stress–strain curve do not cause remarkable internal force redistribution that would affect the overall structural response. Hence, the assumption on linear elasticity used in the derivation of (29) does not cause inaccuracies, but special attention must be paid to the determination of the limit stress values. This topic is discussed in more detail in the next chapter.

4. Validation of the method

4.1. Test series 1 [17]

The proposed method is validated considering the axially loaded CLT panel test series reported in [17]. In total, 12 five-layer simply supported CLT beams were tested under concentric and eccentric loading conditions with the test set-up similar to Fig. 2. The test panels were supplied by two manufacturers in Canada, denoted as Nor and Cor, respectively. The CLT grade was E1 according to the North American CLT product standards [19]. The longitudinal layers were Spruce-Pine-Fir machine-

stress-rated lumber of 1950f-1.7E grade, whereas the transverse layers were No.3 grade. The mechanical properties, such as modulus of elasticity, tensile strength, and compressive strength of the longitudinal lumber, were tested according to the test standards [20]. The compression shear test [21] was implemented to measure rolling shear strength and modulus. No differences from the nominal dimensions nor initial imperfections at the mid-span were reported. The material data for the tests are shown in Table 2.

It should be noted that the rolling shear modulus value 336 MPa, which was obtained from the compression shear tests, is remarkably larger compared to the test results reported, e.g., in [22]. In [17], the compression and tension strengths were measured by using a specially chosen flawless small test specimen, and the obtained average values were 37 MPa and 46 MPa, respectively. To account for the structural anomalies present in larger sized wooden structures, we used a coefficient of 0.8 to convert the small-scale elastic limits to computational elastic limit values.

The experimental test series contained six beams from both manufacturers, which were all loaded axially up to failure. The beam pairs were loaded by using the eccentricities $e = 0, h/6, h/3, h/2, 3h/4$, and h, in which h is the height of the beam cross-section.

Let us consider first the concentric load case in which $e = 0$. With the chosen beam configuration, the beam fails via elastic buckling due to relatively high slenderness. The buckling load of the simply supported beam with the slip-free boundary condition can be calculated using the proposed approach by noting that the function $v(x) = \sin(m\pi x/L)$ is a non-trivial solution satisfying all the boundary conditions. Moreover, due to the fact that there are no transverse loads across the beam length, only the homogenous differential equation part should be considered. Substituting the kinematically feasible displacement function $v(x) = \sin(m\pi x/L)$ in the homogenous differential equations yields

$$B_0 B_s \frac{m^6 \pi^6}{L^6} + (Bk + NB_s) \frac{m^4 \pi^4}{L^4} + Nk \frac{m^2 \pi^2}{L^2} = 0, \qquad (30)$$

from which the critical compression load can be solved in the form [14]

$$N_{cr} = \min_m \frac{B_0 B_s \frac{m^4 \pi^4}{L^4} + Bk \frac{m^2 \pi^2}{L^2}}{B_s \frac{m^2 \pi^2}{L^2} + k}. \qquad (31)$$

By varying the integer m in (31), the lowest value representing the buckling load N_{cr} can be found. Using the data in Table 2, the result is $N_{cr} = 599$ kN with $m = 1$. With this axial compression force value, the compression stress is 28.5 MPa in each parallel layer, being well below the compression strength 0.8*46 = 36.8 MPa. The test results with the concentric loads were 528 kN and 552 kN for manufacturers Nor and Cor, respectively. Hence, the calculated buckling load is 11 % larger than the mean of the two ultimate test loads in the concentric loading condition. For the boundary condition assuming that the slip between faces is prevented at the ends of the beam, the result is $N_{cr} = 600$ kN.

Let us then consider the eccentric loading cases in which the ultimate failure occurs due to exceeding the limit stress in the outermost lamellae. The ultimate axial loads are calculated using the equations given in Chapter 2, supposing that there is no slip at the supports. In the tests, the CLT ends were connected to steel brackets with four 19 mm bolts, which prevents the slip at the beam ends. In all the cases, the compression stresses were critical. The results are given in Table 3

Table 2

Material properties and tested beam dimension according to [17].

$h_i = h_j$ (mm)	h (mm)	b (mm)	L (mm)	E_i (MPa)	Tensile elastic limit (MPa)	Compression elastic limit (MPa)	Rolling shear strength (MPa)	G_j (MPa)
35	175	200	3600	11,465	0.8*37	0.8*46	1.12	336

Table 3

Calculated and experimental failure loads.

Eccentricity (mm)	N_u (kN), mean value of two tests	N_u (kN), the analytical formula, Eq.(29) in [17]	Difference to the tests (%)	N_u (kN), the proposed TLB-based method	Difference in the tests (%)
0	540.5	–	–	600	10.99
h/6 = 29.17	311	311	0	292.76	−5.86
h/3 = 58.33	216.5	196	−9.47	217.05	0.25
h/2 = 87.50	192	152	−20.82	175.20	−8.75
3 h/4 = 131.25	142	122	−14.08	137.17	−3.40
h = 175.00	110	107	−2.73	113.24	2.95

Table 4

Axial stresses at the mid-span, five-layer beam.

Eccentricity (mm)	N_u (kN), proposed method	Compressive stresses (MPa)	Tensile stresses (MPa)
0	600	28.50	–
h/6 = 29.17	292.76	36.80	8.92
h/3 = 58.33	217.05	36.80	16.12
h/2 = 87.50	175.20	36.80	20.11
3 h/4 = 131.25	131.17	36.80	23.73
h = 175.00	99.05	36.80	26.02

including the analytical results of [17] as well as in Fig. 3 including also results according to the Ayrton-Perry buckling curve method [2].
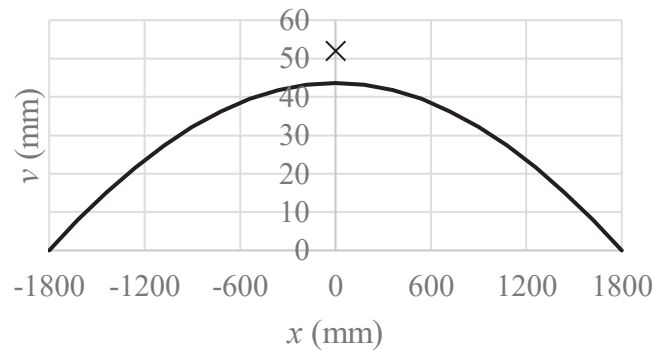
The same eccentrically loaded test cases were calculated also by using the slip-free boundary condition, and the results changed less than 1 % of the values reported in Table 3. This means that the boundary condition associated to the slip between faces, do not have much effect to the forces and stresses near the mid-span of the beam. They have effect to the shear stresses near the supports, as is shown later.

It is seen that the analytical formula given in [17] results in lower values of the ultimate loads than the test values, meaning safe values in all cases. The proposed method gives buckling load values that are both on the safe and unsafe side. In the eccentric cases, the differences between the experimental test results and the proposed method are in the range of (−8.75 %, …, +2.95 %), in which the minus sign means the safe side. The maximum compression and tensile stresses in the analyzed cases are given in Table 4, showing that the failure occurs in each test by the compression stress exceeding the associated limit value, as reported also in [17].

In Figs. 4–6, the deflections as well as the bending moment and shear force distributions in the beam lamellae are highlighted for the case in which eccentricity $e = h/2$ and the axial load reaches the ultimate value 175.20 kN.

Fig. 4. Beam deflection for the case e = h/2, N = 175.20 kN, solid line denotes the calculated result and mark 'x' denotes the experimental result.

As seen in Fig. 5, the moment M_s is taking almost all of the total bending moment M, and the sum of the moments of parallel layers M_0 remains very small, meaning that the axial forces of the parallel layers carry most of the loading. The calculated bending moment M at the mid-span obtains the same value as the moment of external loads (axial force multiplied by the given eccentricity and deflection), ensuring that the calculated stresses and deflections are consistent with the equilibrium equations. Similarly, as shown in Fig. 6, the shear forces, and thus also the shear stresses in the transverse layers Q_s, are very small when
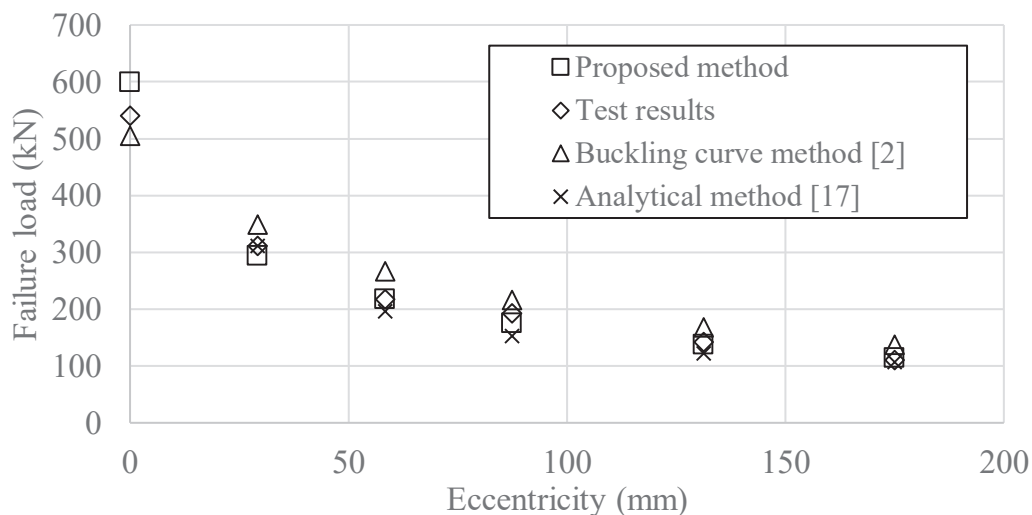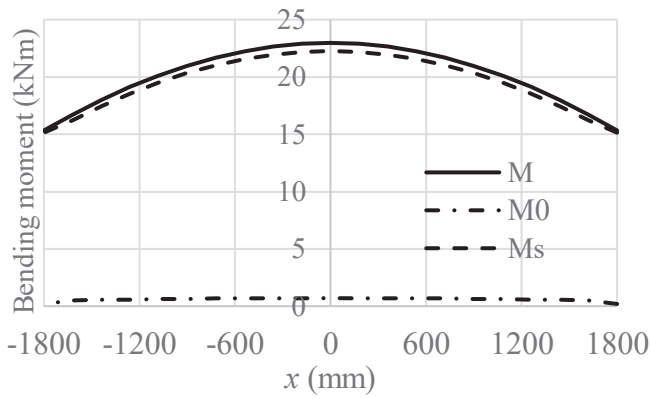
Fig. 3. Calculated and experimental failure loads.

Fig. 5. Calculated bending moments, e = h/2, N = 175.20 kN. M_0 denotes the moment due to the local bending of parallel layers, M_s is the moment due to cross-section bending, and $M = M_0 + M_s$.

approaching the beam ends. Figs. 7 and 8 show a similar phenomenon, but for shear stresses. Fig. 7 also highlights how the boundary condition choice associated with the slip affects the results. Figs. 9 and 10

highlight the bending and shear stress distributions through the cross-section depth at mid-span and at the end of the beam, respectively.

Figs. 7 and 8 highlight the shear stress concentrations near the supports. It is worth noting that the shear stresses in the transverse layers are not close to the respective rolling shear strength values justifying the assumption of elastic stresses.

4.2. Test series 2 [18]

Altogether 15 tests with concentrically and eccentrically loaded CLT panels reported in [18] are utilized for further validation of the proposed method. Due to the fact that the report [18] does not contain the material properties of the timber used, the material data given in Table 2 is adopted for the test series, which is called E1 in the report [18]. This assumption is based on the fact that the material producer for the test series E1 and the tests conducted in [17] is the same. The thicknesses of the specimen and the initial deflections at the mid-sections are measured and reported in [18] and rewritten in Table 5. The remaining seven tests called V1 in [18] are not analyzed because the material property data are not given. Calculated ultimate failure loads based on the proposed theory are reported in Table 6 augmented with failure load value estimations based on the analytical formula derived in [17]. The values e_0 in
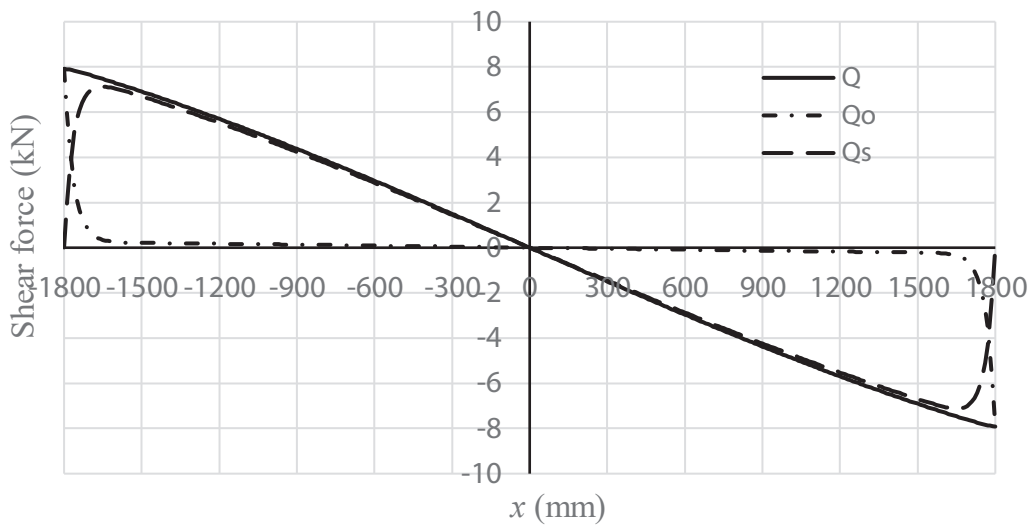

Fig. 6. Calculated shear forces, e = h/2, N = 175.20 kN. Q_0 and Q_s denote the shear forces in parallel and transverse layers, respectively.
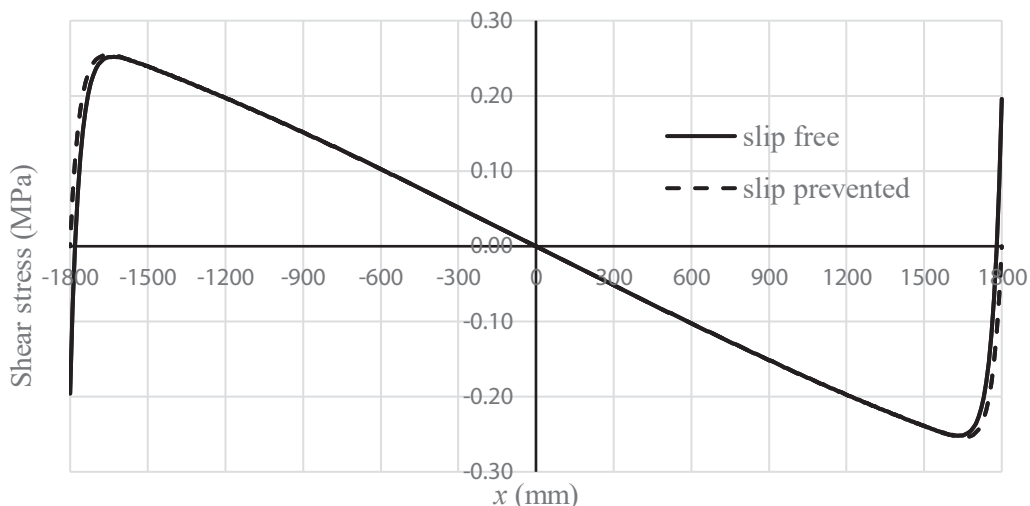

Fig. 7. Calculated shear stresses of transverse layers. The dotted line denotes the slip-prevented boundary condition.
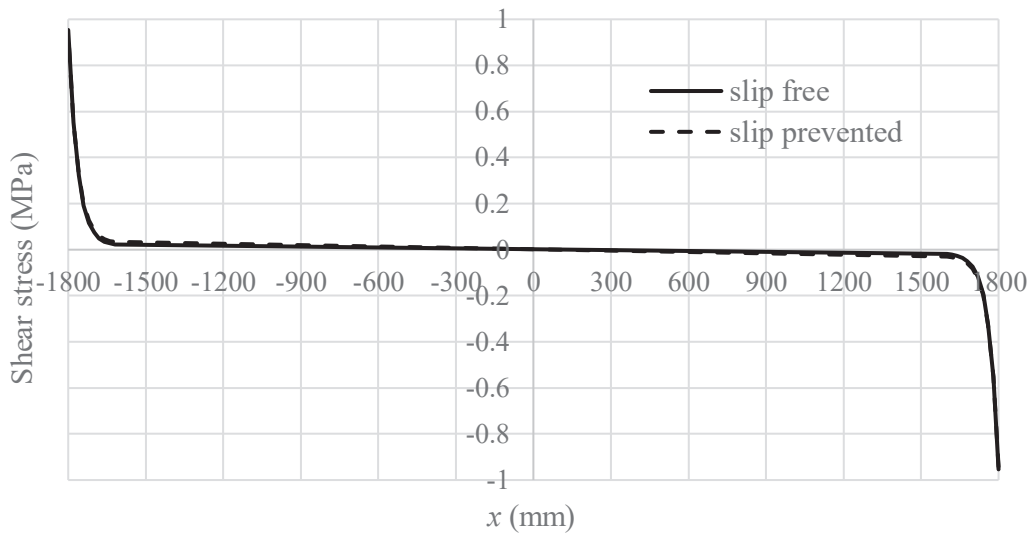
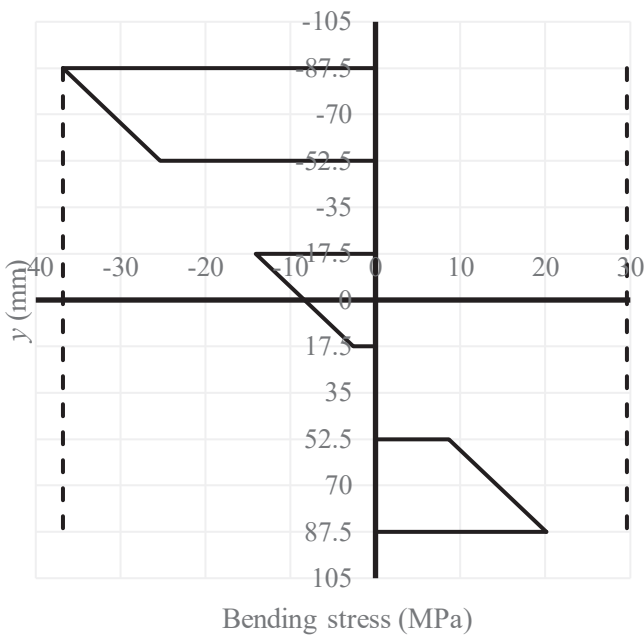**Fig. 8.** Calculated maximum shear stress τ_1 in the outmost parallel layers.

Fig. 9. Calculated bending stress at the mid-span. Vertical dashed lines denote the compression and tension limits.
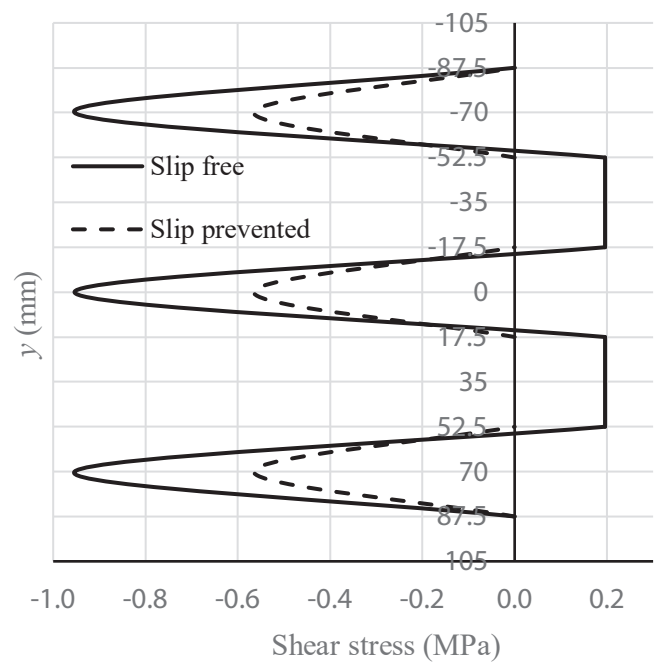

Fig. 10. Calculated total shear stresses at the end of the beam.

Table 5 includes the sums of the eccentricities and the initial deflections.

The proposed method gives results that are on the safe side in all cases, whereas the analytical formula given in [17] estimates the ultimate loads with bigger errors and gives highly unsafe estimations in two cases. In the case E1-T2, the experimental test result for the ultimate failure load is 1046 kN, which is essentially higher than the elastic buckling load. Using the layered beam theory, the buckling load value is 415 kN, and using the proposed method with stress constraints (29), the ultimate failure load value of 384 kN is obtained. The reported experimental ultimate load value 1046 kN is unexpectedly high, but no further explanation for the test result is given in [18].

5. Conclusions

In-plane compression-dominated load cases are typical for CLT walls, and the associated simplified structural design methods are available in design guides. However, the determination of the ultimate load-carrying capacity of such structures is a complex problem, and only a few suitable analytical methods are presented in the literature.

The classical theory of layered beams offers a very attractive theoretical basis for the analysis of CLT structures because the transverse layers with low rolling shear stiffness can be modeled as continuous connection layers. In this paper, the classical theory of layered beams is applied to the structural analysis of compressed CLT panels, and based on the theory, a new analysis method for the ultimate load estimation is proposed.

The proposed method is validated by using two separate test series results presented in the literature [17,18]. As a summary, the proposed method is found to estimate the ultimate failure load accurately both in cases with ideally concentric axial loading as well as in cases in which the axial loading had a certain eccentricity. The tendency in the proposed method results is such that in almost all eccentric cases, the

Table 5

Test data and test results of test series E1 in [18].

Test	Number of layers	$h_i = h_j$ (mm)	h (mm)	b (mm)	L (mm)	e_0 (mm)	N_u tests (kN)
E1-T1	7	34.43	241	600	3600	1.5	3118
E1-T2	3	33.33	100	600	3600	3.0	1046
E1-T3	7	34.43	241	600	3600	84.0	1044
E1-T4	3	33.33	100	600	3600	40.0	240
E1-T5	7	34.43	241	600	3600	41.5	1447
E1-T6	3	33.33	100	600	3600	21.5	310
E1-T7	3	33.33	100	600	3600	18.0	320
E1-T8	3	33.33	100	600	3600	62.0	240

Table 6

Comparisons between results based on tests, proposed method, and analytical formula derived in [17].

Test	N_u test (kN)	N_u (kN), analytical formula given in [17]	Difference to the tests %	N_u (kN), the proposed method	Difference to the tests %
E1-T1	3118	–	–	2759	−11.51
E1-T2	1046	–	–	384	−63.29
E1-T3	1044	867	−16.95	933	−10.63
E1-T4	240	298	24.17	226	−5.83
E1-T5	1447	1273	−12.02	1325	−8.43
E1-T6	310	482	55.48	280	−9.68
E1-T7	320	548	71.25	294	−8.13
E1-T8	240	211	−12.08	186	−22.50

estimated ultimate load was slightly smaller than the experimental one, and the difference between the results was rather independent of the amount of the eccentricity. In the concentric cases, the difference between the proposed method and experimental results was ca. ± 10 %. Reflecting on the results in terms of the theoretical background of the proposed method, it can be concluded that the proposed method is suitable and rather accurate in the ultimate load estimation of compression-dominated CLT structures. It is evident that the proposed method's suitability as such has its limits when the portion of out-of-plane bending loading increases. In the paper, the axial material properties were used for compression-dominated problems, but for bending-dominated structures, the flexural material properties should be adopted instead. Moreover, augmenting the normal stress constraints with other constraints for rolling shear and other failure modes would also extend the method's applicability.

Declaration of Competing Interest

The authors declare that they have no known competing financial interests or personal relationships that could have appeared to influence the work reported in this paper.

References

[1] Karacabeyli E, Gagnon S, FPInnovations (Institute). CLT Handbook: Cross-laminated timber. Quebec: FPInnovations ebec; 2019.

[2] Borgström E, Fröbel J. The CLT Handbook: CLT structures - facts and planning. Stockholm: Swedish Wood; 2019.

[3] Timoshenko S. On the correction factor for shear of the differential equation for transverse vibrations of bars of uniform cross-section. Phil Mag 1921;41:744–6.

[4] Möhler K. Über das Tragverhalten von Biegeträgern und Druckstäben mit zusammengesetzten Querschnitten und nachgiebigen Verbindungsmitteln. Habilitation: Technische Universität Karlsruhe, Germany; 1956.

[5] Kreuzinger H. Flächentragverke – Platten, Scheiben und Schalen – Berechnungsmethoden und Beispiele. Dusseldorf: Fachverlag Holz; 1999.

[6] Marjanović M, Marković N, Damnjanović E, Cvetković R. Three-dimensional stress analysis and design of cross-laminated timber panels using full-layerwise-theory-based finite element method. Thin-Walled Struct 2020;157:107156.

[7] Heinisuo M, Pajunen S. CLT beam analysis using classical elastic theory of layered beams. Rakenteiden Mekaniikka 2021;54(4). https://doi.org/10.23998/rm.107868.

[8] Chitty L. On the cantilever composed of a number of parallel beams interconnected by cross bars. Phil Mag 1947;38(285):685–99.

[9] Granholm H. Om sammansatta balkar och pelare med särskild hänsyn till spikade träkonstruktioner (On composite beams and columns with particular regard to nailed timber structures). No. 88. Göteborg: Transactions of Chalmers University of Technology; 1949.

[10] Hoff N, Mautner S. Bending and buckling of sandwich beams. J Aeronaut Sci 1948;15(12):707–20.

[11] Parland H. Yhdistettyjen puukannattajien lujuus (Strength of composite wooden structures). Helsinki, 1946.

[12] Pleskov P. Teoriia rascheta dereviannykh sostavnnykh sterzhnei (Theoretical studies of composite wood structures). Moscow, 1952.

[13] Davies J. Lightweight Sandwich Construction. Wiley; 2001.

[14] Stamm K, Witte H. Sandwichkonstruktionen. Berechnung, Fertigung, Ausführung. Wien, New York: Springer-Verlag; 1974.

[15] Heinisuo M. Exact Finite Element Method for Layered Beams. Tampere: Publications 56, Tampere University of Technology; 1989.

[16] Holmberg S, Persson K, Petersson H. Nonlinear mechanical behaviour and analysis of wood and fibre materials. Comput Struct 1999;72:459–80.

[17] Huang Z, Huang D, Chui YH, Shen Y, Daneshvar H, Sheng B, et al. Modeling of Cross-Laminated Timber (CLT) panels loaded with combined out-of-plane bending and compression. Eng Struct 2022;250:113335.

[18] Sultan M, Di Leonardo B, Structural performance evaluation of CLT wall-segment/columns under centric and eccentric loadings, A report to NRC, Canada, Report No. A1-005432.3, June 30, 2015.

[19] American National Standard. ANSI/APA PRG 320-2019, Standard for performance-related cross-laminated-timber. The Engineering Wood Association, Approved Jun. 6, 2020. American National Standard Institution.

[20] American Society for Test Materials (ASTM). Standard test method for small clear specimen of timber, ASTM D143-14.

[21] BS EN 16351. Timber structures – Cross laminated timber – Requirements. London: British Standard Institution; 2015.

[22] Ruan G, Xiong H, Chen J. Bending and Rolling Shear Properties of Cross-Laminated Timber Fabricated with Canadian Hemlock. SDHM 2019;13(2):227–46. https://doi.org/10.32604/shdm.2019.04743.